

# Hydrogen Production by Pyrolysis–Nonthermal Plasma/Catalytic Reforming of Waste Plastic over Different Catalyst Support Materials

Idris Aminu, Mohamad A. Nahil, and Paul T. Williams\*



Cite This: *Energy Fuels* 2022, 36, 3788–3801



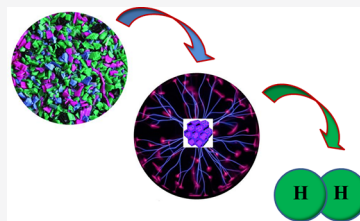
Read Online

ACCESS |

Metrics & More

Article Recommendations

**ABSTRACT:** A two-stage pyrolysis–nonthermal plasma/catalytic steam reforming reactor system was used to produce hydrogen from waste high-density polyethylene in relation to different catalyst support materials. The catalyst support materials investigated were MCM-41, Y-zeolite, ZSM-5,  $\text{Al}_2\text{O}_3$ ,  $\text{TiO}_2$ , dolomite,  $\text{BaTiO}_3$ ,  $\text{CaTiO}_3$ , and  $\text{Mo}_2\text{C}$ . Some of the materials suppressed the generation of plasma, while others enhanced it by improving the generation of microdischarges and surface discharges. Among the tested materials, MCM-41 gave the highest gas yield of 29.2 wt % and a hydrogen yield of  $11 \text{ mmol g}^{-1}_{\text{plastic}}$ . The coupling of the catalyst with the plasma environment resulted in synergy in terms of enhanced total gas yield and hydrogen production, which were higher than those in the absence of plasma (catalyst alone) or plasma alone (no catalyst). Other parameters investigated using the MCM-41 support size and the catalyst bed depth affected the plasma discharge and the total gas yield. Impregnating nickel (10 wt %) on the MCM-41 support further enhanced the total gas yield to 33.3 wt % and the hydrogen yield to  $18 \text{ mmol g}^{-1}_{\text{plastic}}$  due to increased surface reactions. The 10 wt % Ni/MCM-41 was stable when subjected to a 3 h stability test showing no significant change in the yield of the gases.



## 1. INTRODUCTION

The current global production of new plastics is approximately 370 million tons per year with about 60 million tons per year in Europe.<sup>1</sup> Plastic products have a service life ranging from less than a year to over 50 years depending on the plastic type and applications. At the end of their lifetime, the plastic products can have a negative impact on the environment when they enter the waste stream. Generally, all plastics produced globally fall into three fractions: those in use, the collected postconsumer plastic waste, and the noncollected (or mismanaged) plastic waste.<sup>2</sup> In Europe, about 29.1 million tons of postconsumer waste plastics were collected, out of which 32.5% was recycled, 24.9% was sent to waste landfills, and 42.6% was used for energy recovery.<sup>1</sup> There is increasing concern over waste plastics and their impact on the environment.<sup>2,3</sup> For example, the European Union Action Plan for a circular economy introduced a strategy for management of plastics, which aims to curb plastic pollution and its negative impact on the environment.<sup>4</sup> The strategy proposes some measures that encourage industrial process developments and innovations that use waste plastics as feedstocks. The use of waste plastics as feedstocks for useful chemicals such as hydrogen will incentivize the recycling of waste plastics and not only curb the problems caused by the waste plastics but also serve as an alternative source of chemicals, thereby enabling a circular economy.

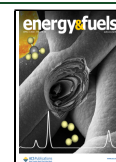
Hydrogen has the potential to become the “fuel of the future” because it is a carbon-free fuel with clean combustion, which could replace fossil fuel usage, thereby reducing  $\text{CO}_2$

emissions and mitigating the effects of climate change. Hydrogen is mainly utilized in the production of ammonia, in oil refining, and in methanol production but with expectations that hydrogen will be in major demand in transportation, industrial energy use, building heat, and power.<sup>5</sup> Therefore, the current hydrogen production of  $\sim 55 \text{ Mt/year}$  is predicted to increase to  $140 \text{ Mt/year}$  by 2050.<sup>5</sup> Hydrogen is mainly produced from fossil fuels and mostly through the steam reforming of natural gas in the presence of a nickel catalyst at around  $800 \text{ }^\circ\text{C}$ . However, alternative nonfossil fuel feedstocks for hydrogen production are under investigation, which will decouple the hydrogen production process from fossil fuels.<sup>6–8</sup> Using waste plastics as an alternative feedstock for hydrogen production has some advantages in that the plastics are produced from fossil fuels and their conversion to hydrogen goes some way to minimize the use of fossil fuels by “recycling” the hydrogen. The use of waste plastics for hydrogen production has been studied by researchers using thermochemical methods such as pyrolysis coupled with catalytic steam reforming. The process uses a two-stage reactor system to produce hydrogen gas from waste

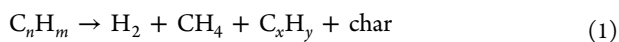
Received: December 9, 2021

Revised: February 28, 2022

Published: March 9, 2022



plastics in a process that mimics the commercial natural gas steam reforming process.<sup>9–12</sup> In the two-stage reactor, the waste plastics are pyrolyzed in the first stage at around 500 °C in an inert atmosphere to produce hydrogen and a range of hydrocarbons (eq 1), plus negligible amounts of char. The volatile gas products then pass to the second-stage reactor where steam reforming of the hydrocarbons takes place in the presence of a catalyst at around 800 °C to produce a hydrogen-rich syngas (eq 2).



Reviews of hydrogen production from waste plastics<sup>13,14</sup> have shown that several researchers have reported a high yield of hydrogen by using the two-stage pyrolysis–steam reforming process;<sup>15</sup> the influence of process conditions, the type of reactor, and the type of catalyst was reported to affect the hydrogen yield.<sup>14</sup>

We have reported on an alternative reactor system, which uses two-stage pyrolysis coupled with nonthermal plasma/catalysis at low temperatures.<sup>15</sup> The nonthermal plasma/catalyst environment is highly reactive but operates at low temperatures, typically less than 250 °C. In a nonthermal plasma, reactive species such as radicals, ions, excited atoms, and molecules are generated at low temperatures from the collision of the reactant molecules and energetic electrons. These reactive species can initiate reactions that are thermodynamically unfavorable at low temperatures.<sup>16</sup> Moreover, coupling the plasma with a catalyst can generate a synergy and improve the energy efficiency and product selectivity.<sup>15,17</sup> The nonthermal plasma can activate the catalyst and modifies the catalyst properties such as the dielectric constant, surface faceting, and morphology, while the catalyst can enhance the generation of reactive species in the plasma.<sup>18</sup> The low operating temperature also reduces the chances of sintering and coking of the catalyst.

Our previous work<sup>15</sup> investigated the influence of different metal–alumina catalysts (Ni, Fe, Co, and Cu) on the yield of hydrogen from the pyrolysis–plasma/catalytic steam reforming of high-density polyethylene. By minimizing or eliminating the high temperature requirement for catalytic reforming, the nonthermal plasma has potential as a technique to reform pyrolysis gases obtained from pyrolysis of waste plastics in a lower-energy and low-cost manner. However, the maximum hydrogen yield from that work was disappointing at only 4.56 mmol g<sup>-1</sup><sub>plastic</sub>. Pyrolysis of waste plastics coupled with conventional thermal catalytic steam reforming has produced much higher yields of hydrogen. For example, reported hydrogen yields from the two-stage pyrolysis catalytic steam reforming of waste plastics range from 66 to 185 mmol g<sup>-1</sup><sub>plastic</sub> depending on the type of plastic investigated, the reactor configuration used, and the process conditions.<sup>19–22</sup> One key factor in enhancing the hydrogen yield in the plasma/catalyst system is the type and composition of catalyst used, which should be designed based on the unique plasma/catalytic reaction environment. Important for the development and enhancement of the plasma are the dielectric constant of the catalyst support materials and the presence of metal species on the catalyst surface and within pores. Such factors promote plasma formation and promote the catalyst reforming activity and selectivity for hydrogen production in the plasma environment. Fewer catalysts have been studied for the

plasma/catalytic reforming process compared to conventional thermal catalytic reforming, and there has been inconsistency in the results with some showing synergy and some reporting otherwise. For example, Wang et al.<sup>18</sup> reported a decrease in the conversion of CH<sub>4</sub> and CO<sub>2</sub> to liquid fuels and chemicals when metal–alumina catalysts were used in the discharge zone of a plasma/catalytic reactor compared to when plasma alone was used. However, Chen et al.<sup>23</sup> reported significant improvement in the catalytic methanation of CO<sub>2</sub> when a zeolite catalyst was introduced into the plasma/catalyst reactor system. Similarly, introduction of a Ni/Al<sub>2</sub>O<sub>3</sub> catalyst into the plasma zone enhanced the catalytic synthesis of ammonia in a plasma/catalyst reactor.<sup>24</sup> This suggests that the plasma interacts differently with different catalysts, and therefore, more work is needed to fully understand the selection of the catalysts for highly efficient plasma/catalytic reforming and also the synergistic effect of plasma/catalysis.<sup>25</sup> Similar to the thermal catalytic reforming, Ni supported on Al<sub>2</sub>O<sub>3</sub> has been the most studied catalyst for the plasma/catalytic reforming.<sup>26</sup> However, the most effective materials used for thermal catalysis may not necessarily be the most effective for plasma/catalysis, and thus, there is a need to investigate more materials for plasma/catalysis.

The choice of a suitable support for the catalyst is important because supports stabilize the metal particles by allowing the physical separation of the small metal crystallites, thereby avoiding their agglomeration into larger crystallites.<sup>27</sup> The characteristics of the catalyst such as the porous structure, surface area, metal–support interaction, size of metal crystallites, mechanical strength, and chemical properties, which affect the catalytic activity, are all influenced by the type of support used.<sup>28</sup> Sintering of the catalyst, which increases carbon formation, has been shown to be reduced by strong metal–support interactions.<sup>29</sup> These properties consequently affect the interaction of the plasma and the catalyst and catalyst stability in the plasma/catalysis reactions. Different catalyst support materials have been investigated for plasma/catalysis reactions. For example, Azzolina-Jury et al.<sup>30</sup> reported the activity of two different zeolite supports (ZSM-11 and USY), with different Ni contents and Si/Al molar ratios, in the plasma/catalytic hydrogenation of CO<sub>2</sub> in a packed-bed catalytic reactor. They reported that the type of zeolite structural catalyst framework and the Si/Al molar ratio affect the activity of the catalysts in the reaction. CO yield and selectivity followed the trend ZSM-11 (5 wt % Ni) > ZSM-11 (2.5 wt % Ni) > USY (30) > USY (40), while an inverted trend was observed for CH<sub>4</sub> yield. Mei et al.<sup>31</sup> studied the influence of four different nickel catalysts with different support materials (Ni/Al<sub>2</sub>O<sub>3</sub>, Ni/SiO<sub>2</sub>, Ni/MgO, and Ni/TiO<sub>2</sub>) for the plasma/catalytic reforming of biogas and reported the Ni/Al<sub>2</sub>O<sub>3</sub> as the best performing catalyst. Similarly, Khoja et al.<sup>32</sup> investigated the effect of nickel on different supports (Ni/γ-Al<sub>2</sub>O<sub>3</sub>, Ni/MgO, and Ni/γ-Al<sub>2</sub>O<sub>3</sub>-MgO) for the dry reforming of methane (DRM) in a dielectric barrier discharge (DBD). The highest conversion of both CH<sub>4</sub> and CO<sub>2</sub> was obtained with the Ni/γ-Al<sub>2</sub>O<sub>3</sub>-MgO.

Since nickel catalysts have been shown to be highly efficient in their selectivity for hydrogen production,<sup>33–36</sup> the objective of the work reported here is to couple nickel with a highly suitable support material for the plasma/catalysis of HDPE pyrolysis vapors at low temperatures with the aim of increasing hydrogen yield. The novelty of the work lies in developing an understanding of the role of the catalyst support material for

hydrogen production from waste plastics, in the unique process conditions of the plasma/catalyst environment. Nine different materials were investigated with varied surface areas, porosities, and dielectric constants, all factors that influence the development of the plasma and thereby enhance the reforming reactions of hydrocarbons derived from waste plastic pyrolysis to produce hydrogen. The different materials were tested to understand the role of material properties in the plasma/catalysis process. The experimental system consisted of two stages, pyrolysis of the HDPE in the first stage followed by plasma/catalytic reforming in the second stage using a dielectric barrier discharge nonthermal plasma reactor. Nickel was then impregnated on the best performing material and, for comparison, on three other materials, which were then used as catalysts for the reforming reactions. The performance of the different catalysts and supports investigated was in relation to hydrogen production and the total gas yield. The fresh catalysts were characterized using a range of techniques, nitrogen adsorption–desorption, X-ray diffraction (XRD), hydrogen temperature-programmed reduction ( $H_2$ -TPR), and focused ion beam-scanning electron microscopy (FIB-SEM), while the used catalysts were characterized for carbon deposition using temperature-programmed oxidation (TPO).

## 2. MATERIALS AND METHODS

**2.1. Materials.** The waste plastic used was high-density polyethylene (HDPE) obtained as 2 mm pellets of postconsumer recycled waste plastic from Regain Polymers, Castleford, UK. Ultimate analysis showed 81.78% carbon, 10.59% hydrogen, and 0.54% nitrogen. Proximate analysis revealed a moisture content of 0.14%, a volatile matter content of 97.84%, a fixed carbon content of 0.16%, and an ash content of 3.63%. Nine different catalyst support materials, MCM-41, Y-zeolite, ZSM-5, (Nankai University, China), dolomite (Warmsworth Quarry, UK), barium titanate (Catal Int. Ltd., UK), calcium titanate, molybdenum carbide, alumina, and titanium dioxide (Thermo Fisher Scientific, UK), were used to investigate the effect of different materials on hydrogen yield from the plasma/catalytic reforming of HDPE pyrolysis vapors. Since there are few reports on different catalysts used in the reforming plasma/catalysis reaction environment, a starting point for catalyst selection involved screening of a variety of classes of materials, i.e., zeolites, metal oxides, perovskites, oxides, and carbides.

**2.2. Catalyst Preparation.** In addition to the investigation of the influence of the nine different support materials, four selected supports were used with 10 wt % nickel addition: Ni/MCM-41, Ni/BaTiO<sub>3</sub>, Ni/Al<sub>2</sub>O<sub>3</sub>, and Ni/Y-zeolite. These Ni-based catalysts were chosen based on the best performance for the production of hydrogen of the nine different supports and also the most studied reforming catalyst in thermal catalysis (Ni/Al<sub>2</sub>O<sub>3</sub>) and also the material with the highest dielectric constant (BaTiO<sub>3</sub>). Nickel was the chosen active metal since our previous work<sup>15</sup> on pyrolysis–plasma/catalysis of HDPE showed that Ni supported on Al<sub>2</sub>O<sub>3</sub> was clearly the best metal catalyst compared with Fe/Al<sub>2</sub>O<sub>3</sub>, Co/Al<sub>2</sub>O<sub>3</sub>, and Cu/Al<sub>2</sub>O<sub>3</sub> in terms of hydrogen production. A 10 wt % Ni loading was used in each case because this metal loading has been reported to result in reactive sites that are neither deficient of the metal nor saturated by the metal.<sup>15</sup> The Ni-based catalysts were prepared using a wet impregnation method since wet impregnation has been shown to produce good dispersion of nickel on the support material.<sup>19</sup> A measured amount of nickel nitrate was fully dissolved in deionized water, and then, a measured quantity of the support was added and stirred with a magnetic stirrer for 30 min. The mixture was then heated until a slurry was made, which was dried overnight in an oven and then calcined in limited air at 750 °C for 3 h. A calcination temperature of 750 °C was chosen because it is not too low to reduce interactions between nickel and the support and neither is it too high to result in very strong Ni–support interactions that can be unfavorable for reduction of the

catalyst. This was followed by grinding and sieving of the catalyst to obtain a particle size of 50–212 μm, and the catalyst was then reduced in a hydrogen atmosphere (5% H<sub>2</sub> in 95% N<sub>2</sub>) by heating to 800 °C at a heating rate of 20 °C min<sup>-1</sup> and held at 800 °C for 2 h. Catalyst reduction under hydrogen was carried out at 800 °C even though the catalyst held in the DBD plasma/catalyst reactor was at 250 °C for all experiments. This was because we wished to ensure that the catalyst was suitably reduced to ensure comparable reaction conditions to those used in our previous work using high-temperature (>800 °C) thermal pyrolysis–catalytic reforming<sup>9,15,19,20</sup> to allow comparison with such results.

**2.3. Pyrolysis–Plasma/Catalytic Reactor System.** Figure 1 shows a schematic diagram of the experimental pyrolysis–plasma/

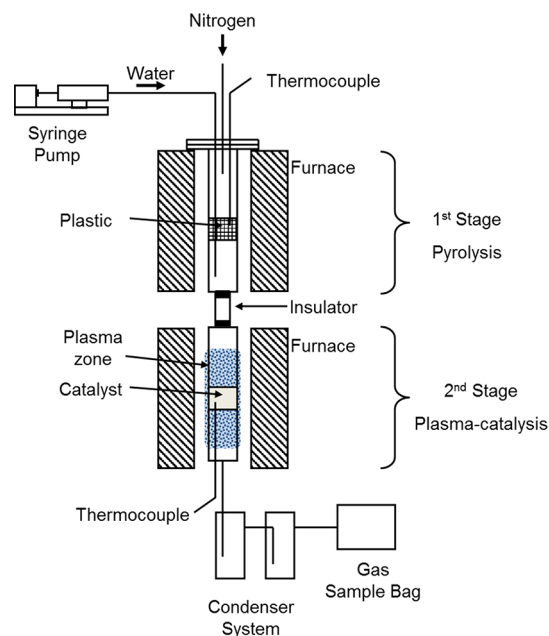


**Figure 1.** Schematic diagram of the two-stage pyrolysis–plasma/catalytic reactor system.

catalytic reactor system. The experimental system and procedure have been described elsewhere<sup>15</sup> but are briefly summarized here. The reactor was a two-stage pyrolysis–dielectric barrier discharge nonthermal plasma/catalyst reactor. Pyrolysis of the HDPE produced volatiles, which passed directly through the plasma/catalytic reactor using a nitrogen purge for steam reforming in the presence of the different catalysts and catalyst support materials. The two-stage reactor was constructed of stainless steel. The HDPE (1.0 g) was loaded into a stainless steel crucible and placed in the center of the pyrolysis reactor. Pyrolysis of the HDPE took place in the first stage using an electrical furnace, which provided heating of the HDPE from 20 to 500 °C at a heating rate of 20 °C min<sup>-1</sup> and was held at 500 °C for 15 min. The catalyst (1.0 g) was held in the discharge gap of the DBD supported by quartz wool at a temperature of 250 °C using an external electrical furnace. The temperature of 250 °C for the DBD reactor furnace was chosen to avoid rapid condensation of the pyrolysis hydrocarbons and/or steam in the plasma/catalyst reactor. The DBD plasma reactor consisted of a quartz tube with an outer copper electrode and an inner aluminum rod, and the catalyst was placed in the gap between the quartz tube inner electrode and the aluminum inner electrode. The plasma was generated between the two electrodes using an AC high-voltage power supply (0–240 V) with a frequency of 1500 Hz and a maximum peak-to-peak voltage of 20 kV while the outer electrode was grounded. Electrical process parameters were monitored using a Tektronix MDO3024 oscilloscope. Steam was introduced into the second-stage plasma reactor using distilled water by a syringe pump at 2 g h<sup>-1</sup>. The outlet of the reactor led to a water and dry-ice condenser system to condense

liquids, and gases were passed to a Tedlar gas sample bag. Product gases were analyzed immediately using packed column gas chromatography using three different Varian CP-3380 gas chromatographs for (i) C<sub>1</sub>–C<sub>4</sub> hydrocarbons, (ii) permanent gases (H<sub>2</sub>, O<sub>2</sub>, N<sub>2</sub>, and CO) and (iii) CO<sub>2</sub>. At the end of the experiment, the residual solid from the pyrolysis reactor was collected along with the condensed liquids trapped in the condensation system and the catalyst from the plasma/catalyst reactor and weighed for the determination of mass closure. The total mass of gas produced was determined from the gas chromatographic data; knowing the N<sub>2</sub> gas flow, experimental time, and gas concentration in the gas sample bag, the mass of other gases could be calculated. Therefore, the total gas yield could be determined by mass rather than “by difference”.

**2.4. Support Material and Catalyst Characterization.** The physicochemical properties of the catalyst support materials were characterized using a range of techniques: X-ray diffraction (XRD), nitrogen adsorption–desorption, temperature-programmed reduction (H<sub>2</sub>-TPR), scanning electron microscopy (SEM), and focused ion beam-scanning electron microscopy (FIB-SEM). The surface area and porosity of the support materials and Ni-based catalysts were determined using nitrogen adsorption–desorption. About 0.2 g of each sample was degassed at a temperature of 200 °C under a nitrogen atmosphere for 12 h, and then, the nitrogen adsorption–desorption isotherms were obtained using a Micromeritics Tristar 3000 instrument. The surface area was obtained by the Brunauer–Emmett–Teller (BET) method while the pore size and the pore volume were obtained by the Barrett–Joyner–Halenda (BJH) method applied on the desorption isotherms. The crystalline structures/phases of the metal catalysts were analyzed using X-ray diffraction (XRD), carried out using a Bruker D8 diffractometer with Cu K $\alpha$  radiation. The diffraction spectra were recorded over a  $2\theta$  range of 10–80° using a scanning step of 0.033, and peaks were identified using the HighScore Plus software package. To understand the effect of the supports on the reduction behavior of the catalyst, H<sub>2</sub>-TPR was carried out in a Shimadzu TGA-50 analyzer using hydrogen gas (5% H<sub>2</sub>/95% N<sub>2</sub>) as the reducing agent. About 25 mg of the calcined catalyst was placed onto an alumina pan and heated under a hydrogen/nitrogen atmosphere from ambient temperature to 850 °C at 20 °C min<sup>-1</sup>. The three-dimensional internal structures of the catalysts were visualized by focused ion beam (FIB)-scanning electron microscopy (SEM) where the FIB was used for the sectioning/milling of the samples and the images of the exposed cross sections were imaged by SEM. The samples were coated with platinum before the milling was carried out then characterized using a FEI Helios G4 CX dual-beam SEM with a precise focused ion beam. The nickel mapping with the SEM was obtained from coupled energy-dispersive X-ray spectroscopy (EDX).

### 3. RESULTS AND DISCUSSION

**3.1. Catalyst Characterization.** The textural, physical, and chemical properties of the investigated support materials and nickel-based catalysts are important because they determine how the materials interact with the reacting pyrolysis gases, which affects the catalyst activity and the consequent production of hydrogen. In addition, the properties of the materials affect how they interact with the plasma, which determines the performance of the plasma/catalytic steam reforming system. Table 1 shows the BET surface area, pore volume, and pore diameter of the catalyst support materials characterized by nitrogen adsorption–desorption.

The MCM-41 support has the largest specific surface area (802 m<sup>2</sup> g<sup>-1</sup>) followed by Y-zeolite (718 m<sup>2</sup> g<sup>-1</sup>), ZSM-5 (317 m<sup>2</sup> g<sup>-1</sup>), Al<sub>2</sub>O<sub>3</sub> (274 m<sup>2</sup> g<sup>-1</sup>), and TiO<sub>2</sub> (161 m<sup>2</sup> g<sup>-1</sup>). These substrates also exhibit high porosity as indicated by the pore volume data. The other materials have a far lower surface area with CaTiO<sub>3</sub>, BaTiO<sub>3</sub>, dolomite, and MO<sub>2</sub>C having surface areas of less than 4 m<sup>2</sup> g<sup>-1</sup>. They are also less porous having

**Table 1. Properties of the Catalyst Support Materials**

| sample                         | S <sub>BET</sub> (m <sup>2</sup> g <sup>-1</sup> ) | pore volume (cm <sup>3</sup> g <sup>-1</sup> ) | pore diameter (nm) |
|--------------------------------|--|--|--------------------|
| MCM-41                         | 802  | 0.851  | 3.36               |
| Y-zeolite                      | 718  | 0.316  | 13.38              |
| ZSM-5                          | 317  | 0.363  | 8.61               |
| Al <sub>2</sub> O <sub>3</sub> | 274  | 0.322  | 5.79               |
| TiO <sub>2</sub>               | 161  | 0.459  | 8.80               |
| CaTiO <sub>3</sub>             | 3.9  | 0.0092   | 22.87              |
| BaTiO <sub>3</sub>             | 2.2  | 0.0034   | 7.71               |
| dolomite                       | 1.5  | 0.0047   | 12.02              |
| MO <sub>2</sub> C              | 0.6  | 0.0006   | 34.71              |

pore volumes less than 0.01 cm<sup>3</sup> g<sup>-1</sup>. Impregnating the supports with nickel significantly reduced the specific surface area and the pore volume of the product catalysts, while the pore diameter of the catalysts increased as shown in Table 2.

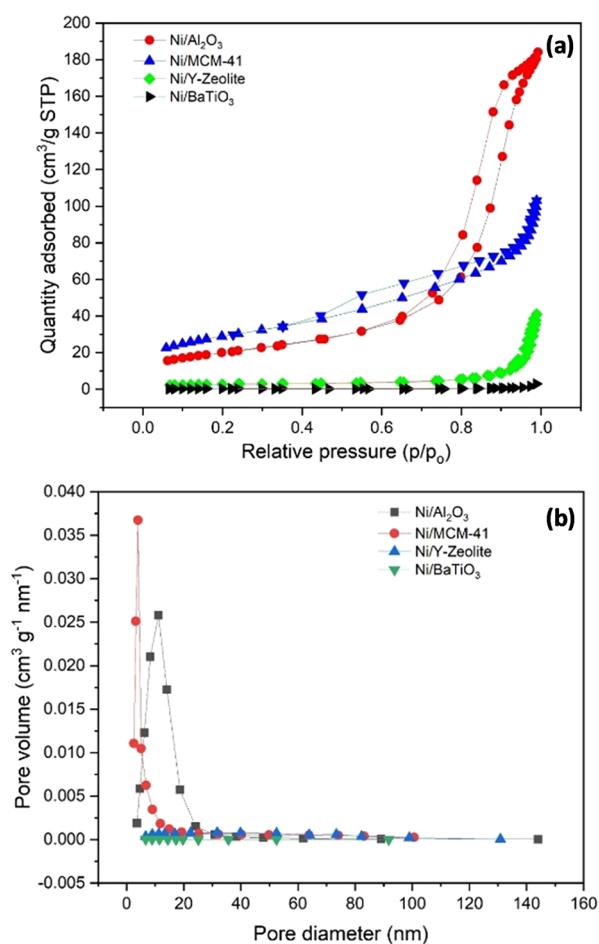
**Table 2. Properties of the Nickel Catalysts**

| sample                            | S <sub>BET</sub> (m <sup>2</sup> g <sup>-1</sup> ) | pore volume (cm <sup>3</sup> g <sup>-1</sup> ) | pore diameter (nm) |
|-----------------------------------|--|--|--------------------|
| Ni/MCM-41                         | 417  | 0.307  | 3.6128             |
| Ni/Y-zeolite                      | 380  | 0.161  | 12.2184            |
| Ni/Al <sub>2</sub> O <sub>3</sub> | 72   | 0.286  | 13.4721            |
| Ni/BaTiO <sub>3</sub>             | 4.3  | 0.006  | 7.1642             |

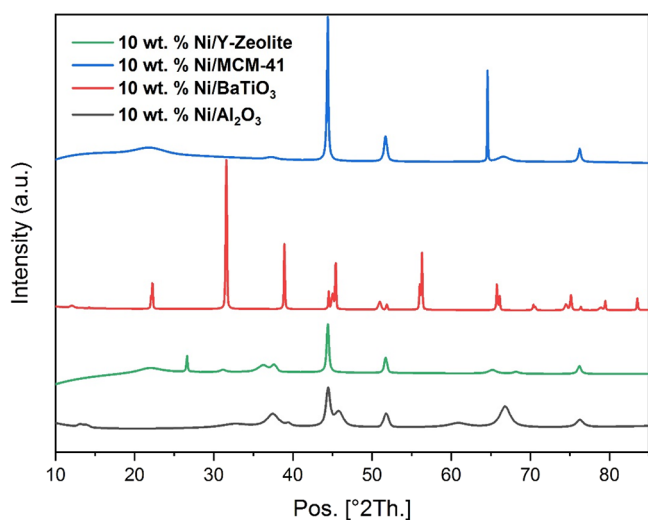
For example, the MCM-41 support material had a surface area of 802 m<sup>2</sup> g<sup>-1</sup> and a pore volume of 0.851 cm<sup>3</sup> g<sup>-1</sup>, whereas the Ni-MCM-41 catalyst had a surface area of only 417 m<sup>2</sup> g<sup>-1</sup> and a pore volume of 0.307 cm<sup>3</sup> g<sup>-1</sup>. The addition of nickel to the support materials resulted in nickel species occupying a large portion of the pores, thus decreasing the surface area of the catalyst and the average pore volume. However, the high calcination temperature used (750 °C) increased the pore diameters of the Ni-based catalysts. Similar observations were made by other researchers.<sup>37,38</sup> In the case of Ni/BaTiO<sub>3</sub>, the surface area increased slightly from 2.2 to 4.3 m<sup>2</sup> g<sup>-1</sup> after the nickel impregnation perhaps because of the large nickel particle size and small existing pores of BaTiO<sub>3</sub> and thereby did not block any pores of BaTiO<sub>3</sub>.

Figure 2a shows the nitrogen adsorption–desorption isotherms obtained at 77 K for the different nickel-based catalysts. The isotherms for all the catalysts are of type IV with type H1 hysteresis for Ni/Al<sub>2</sub>O<sub>3</sub>, while the other three depict type H3 hysteresis. According to IUPAC classification, this indicates that the Ni/Al<sub>2</sub>O<sub>3</sub> is a mesoporous material consisting of uniform spherical structures in regular arrangement, while Ni/MCM-41, Ni/Y-zeolite, and Ni/BaTiO<sub>3</sub> have a mesoporous structure with interconnected pores, and the adsorption is via multilayer adsorption and capillary condensation.<sup>39</sup> The pore size distribution derived from the desorption isotherm is presented in Figure 2b. The figure shows that a high-volume uptake of nitrogen by all the catalysts was observed at pore sizes between 2 and 50 nm, which confirmed the mesoporous structure of the catalysts.

The crystallographic characterization of the prepared Ni-based catalysts was determined using XRD. Figure 3 shows the XRD spectra of the four different nickel catalysts with the different support materials, where peaks corresponding to crystalline elemental nickel and the supports were observed. For all the catalysts, no NiO was observed because it had been reduced to elemental nickel through reduction in the catalyst preparation stage. Peaks corresponding to nickel were observed



**Figure 2.** (a) Nitrogen adsorption–desorption isotherms and (b) pore size distributions of the prepared catalysts.



**Figure 3.** XRD spectra of the different nickel-based catalysts.

in all the catalysts at positions of  $2\theta = 44.5$  and  $51.7^\circ$ . A high interaction between the metal and the support was evidenced by the formation of nickel aluminate spinel peaks at  $65.5^\circ$  for all of the nickel-based catalysts. Diffraction peaks for Ni/BaTiO<sub>3</sub> at  $2\theta = 31.5$ ,  $38.9$ , and  $56.3^\circ$ , which are assigned to BaTiO<sub>3</sub>, show that the BaTiO<sub>3</sub> structure remains in the catalyst implying weak metal–support interactions. This is supported

by TPR data that shows a lower reduction at lower temperatures suggesting weak interactions between the catalyst support and Ni.

The effect of the different support materials on the reducibility and metal–support interactions of the nickel catalysts was investigated using H<sub>2</sub>-TPR, and the reduction profile is presented in Figure 4. The reduction corresponding

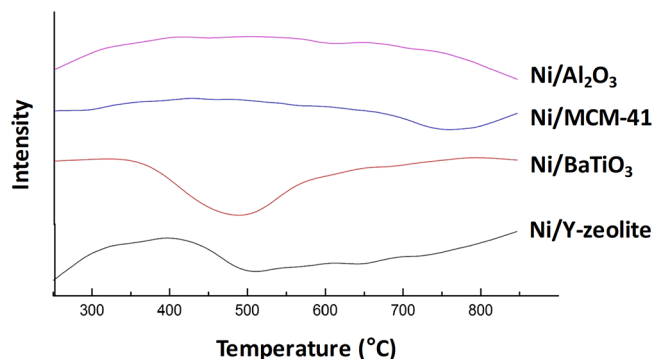


**Figure 4.** H<sub>2</sub>-TPR of the different nickel-based catalysts.

to the conversion of the supported NiO to metallic nickel was observed for all the catalysts. The results showed that the nickel metal interacted differently with the different supports. For the Ni/Y-zeolite catalyst, reduction started at a temperature of  $\sim 700^\circ\text{C}$ , and the maximum weight loss observed was at a temperature of  $\sim 850^\circ\text{C}$ . On the other hand, Ni/BaTiO<sub>3</sub> was easily reduced, starting at a much lower temperature of  $\sim 500^\circ\text{C}$  with a reduction peak at around  $570^\circ\text{C}$ . The relatively larger nickel particle size reported for the BaTiO<sub>3</sub> support made reduction easier than the other catalysts.<sup>40</sup> The reason is suggested to be due to the lower interaction between the nickel particles and the BaTiO<sub>3</sub> support. However, reduction of the 10 wt % Ni/Al<sub>2</sub>O<sub>3</sub> and Ni/MCM-41 catalysts started at a temperature of  $\sim 800^\circ\text{C}$  suggesting a stronger metal–support interaction than the other catalysts, which may be due to the reduction of nickel aluminate spinel.<sup>41</sup> The presence of the nickel aluminate spinel was observed for both Ni/Al<sub>2</sub>O<sub>3</sub> and Ni/MCM-41 in the XRD spectrum. Richardson and Twigg<sup>42</sup> suggested that impregnating Al<sub>2</sub>O<sub>3</sub> with Ni(NO<sub>3</sub>)<sub>2</sub> gives an acidic environment that dissolves Al<sup>3+</sup> ions on the Al<sub>2</sub>O<sub>3</sub> surface. The NiO crystals decomposed during the thermal treatment of the catalyst, they interacted with the Al<sup>3+</sup> ions by incorporating the ions into the crystallite structure, or the ions accumulated in the immediate vicinity of the crystals resulting in a decrease in the reducibility of the catalyst.

**3.2. Hydrogen Production from Pyrolysis–Plasma/Catalytic Steam Reforming.** The effects of different types of support materials and nickel-supported catalysts on the yield of hydrogen from nonthermal plasma reforming of waste high-density polyethylene (HDPE) pyrolysis products were investigated using the two-stage pyrolysis–catalytic steam reforming reactor system. The performance of the catalysts was assessed based on the total gas yield, syngas (H<sub>2</sub> and CO) and hydrogen yield, and the amount of carbon deposition on the catalyst surface.

**3.2.1. Influence of Different Catalyst Support Materials.** The different catalyst materials investigated were MCM-41, Y-zeolite, ZSM-5, dolomite, alumina, barium titanate, calcium titanate, titanium dioxide, and molybdenum carbide. The experiments on the pyrolysis–plasma/catalytic steam reform-

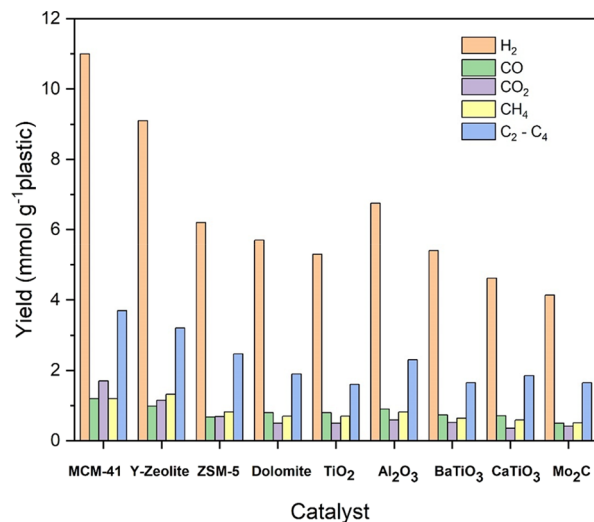
**Table 3. Product Gas and Liquid Yield from the Pyrolysis-Plasma/Catalytic Steam Reforming of HDPE in Relation to Different Catalyst Support Materials**

| product yield (wt %) | catalyst support material |           |       |          |                                |                    |                    |                   |                  |
|----------------------|---------------------------|-----------|-------|----------|--------------------------------|--------------------|--------------------|-------------------|------------------|
|                      | MCM-41                    | Y-zeolite | ZSM-5 | dolomite | Al <sub>2</sub> O <sub>3</sub> | BaTiO <sub>3</sub> | CaTiO <sub>3</sub> | MO <sub>2</sub> C | TiO <sub>2</sub> |
| gas                  | 29.2                      | 26.7      | 17.0  | 13.6     | 16.5                           | 12.7               | 12.5               | 11.2              | 12.9             |
| liquid               | 157.3                     | 159.8     | 160.6 | 166.1    | 162.4                          | 181.9              | 179.8              | 201.4             | 177.3            |

ing of HDPE for hydrogen production in relation to the different support materials were carried out at a pyrolysis temperature of 500 °C, and plasma/catalysis was carried out at a controlled DBD reactor temperature of 250 °C. A plasma power input of 80 W was used to sustain the plasma discharge in the DBD reactor, and steam reforming was carried out with steam injected at a rate of 2 g h<sup>-1</sup>. The effectiveness of the different catalyst materials was compared based on the total product gas yield and hydrogen yield. The mass of liquid that comprised the product pyrolysis oil and unreacted water was recorded but not analyzed. The solid char residue yield collected from the pyrolysis reactor remained at ~4 wt % for each of the experiments because the same mass of HDPE was used throughout. Virgin HDPE is known to produce no solid char during pyrolysis, where only volatiles are produced.<sup>43</sup> However, the HDPE used in this work was recycled postconsumer plastic and would typically contain additives used in the manufacture of the HDPE required for the various consumer products, such as antioxidants, fire retardants, inorganic filler materials, etc., which would contribute to the production of char. Different hydrogen yields were obtained when the different materials were used depending on their interaction with the plasma for cracking the pyrolysis volatiles into syngas and lower hydrocarbons (C<sub>1</sub>–C<sub>4</sub>). The product gas and liquid yield obtained from the experiments are presented in Table 3. The results are calculated on the basis of input plastic and water (steam) and output product gas, liquid (oil + unreacted water) and char yield. However, some of the input water will contribute to steam reforming reactions to generate gas. When the data is calculated on the basis of input mass of plastic alone, the material balance will be well in excess of 100 wt.%.

The highest total gas yields, by a significant margin, were obtained with the MCM-41 and Y-zeolite support materials from the pyrolysis–plasma/catalytic reforming of HDPE at 29.2 and 26.7 wt %, respectively (Table 3). This is an indication that the combination of the plasma with the MCM-41 and Y-zeolite resulted in a more enhanced electric field that cracked more of the HDPE pyrolysis volatiles to produce gases. The high surface areas of the MCM-41 (802 m<sup>2</sup> g<sup>-1</sup>) and Y-zeolite (718 m<sup>2</sup> g<sup>-1</sup>) contributed to their effectiveness in cracking the high-molecular-weight pyrolysis volatiles into lower-molecular-weight hydrocarbons, which were then reformed into syngas (H<sub>2</sub> and CO). The order of the catalyst support materials in terms of the influence on total gas yield was MCM-41 > Y-zeolite > ZSM-5 > alumina > dolomite > TiO<sub>2</sub> > BaTiO<sub>3</sub> > CaTiO<sub>3</sub> > Mo<sub>2</sub>C.

Figure 5 shows the gas composition derived from the pyrolysis–plasma/catalysis of HDPE using the different support materials. In each case, syngas (H<sub>2</sub> and CO) was produced from the steam reforming of the hydrocarbon pyrolysis volatiles (eq 1), while the presence of CO<sub>2</sub> suggested that the water gas shift reaction (eq 2) also occurred. Hydrogen was the major gaseous product followed by the C<sub>2</sub>–C<sub>4</sub> hydrocarbons. In a plasma/catalysis system, the

**Figure 5.** Gas composition from pyrolysis–nonthermal plasma reforming of waste HDPE using different catalyst support materials.

interaction of the plasma with the catalyst material can change the type of plasma discharge and may enhance or reduce the electric field.<sup>16,44</sup>

Figure 5 shows that the highest hydrogen yield of 11 mmol g<sup>-1</sup> plastic was obtained when MCM-41 was used as the catalyst material followed by Y-zeolite at 9.1 mmol g<sup>-1</sup> plastic. Significantly lower hydrogen yields were obtained from the other catalyst support materials. MCM-41 and Y-zeolite also produced higher yields of CO at 1.2 and 1.0 mmol g<sup>-1</sup> plastic, respectively, which shows that they were both more active in the low-temperature nonthermal reforming of the waste HDPE volatiles compared to the other catalyst support materials. The different performances by the different packing materials can be partly attributed to the different discharge characteristics when the packing materials are loaded in the discharge region.

There are several factors that made MCM-41 and Y-zeolite have a more effective performance for hydrogen production among the nine packing materials used in this study. One of the factors is the surface area of the materials used. MCM-41 had the highest surface area. In plasma/catalysis, the discharge changes from a filamentary discharge to a combination of microdischarges and surface discharges on the catalyst surface with most of the discharge being on the surface of the catalyst.<sup>45</sup> Therefore, more surface discharges are produced on the catalyst with a higher surface area resulting in more cracking of the tar. Comparing MCM-41, Y-zeolite, and ZSM-5, which have the same chemical elements but different surface areas, show that the surface area is crucial in the performance of the material in the plasma/catalysis reactions.

Another contributory factor to enhanced hydrogen yield in the plasma/catalytic system is the dielectric constant of the different materials. The dielectric constant refers to the induced polarization stored in a certain volume of the catalyst support material when an electric field is applied and

represents the stored potential energy.<sup>46</sup> Thereby, low-dielectric-constant materials promote more microdischarges compared to high-dielectric-constant materials. The zeolites have a dielectric constant lower than 5, TiO<sub>2</sub> has a dielectric constant in the range of 40–100, while the dielectric constant of Al<sub>2</sub>O<sub>3</sub> is 8–11. The dielectric constant of dolomite is low at 8.5<sup>47</sup> and would be expected to enhance the plasma, but the surface area is very low at 1.5 m<sup>2</sup> g<sup>-1</sup>, and the porosity is also low. The ferroelectric materials, CaTiO<sub>3</sub> and BaTiO<sub>3</sub>, have very large dielectric constants of 200 and 10,000, respectively. The materials with higher dielectric constants such as BaTiO<sub>3</sub> and CaTiO<sub>3</sub> gave a poorer performance in terms of hydrogen yield in the plasma/catalytic reforming reactions. Interactions of the nonthermal plasma with these high dielectric materials resulted in a lower effective electric field and a low electron energy, which is not strong enough to crack most of the derived pyrolysis hydrocarbons. Patil et al.<sup>48</sup> suggested that when an electric field is applied to a material with a high dielectric constant, the material easily becomes polarized. The polarized material then creates an internal electric field that opposes the overall electric field resulting in a decrease in the energy of electrons; the implication is that this results in decreased energy of the reactive species and decreased gas ionization. Kim and Ogata<sup>49</sup> compared discharges observed using an ICCD camera in a discharge barrier packed with zeolites and with BaTiO<sub>3</sub>. They observed that surface plasma discharge streamers appeared on the surface of the zeolite-packed plasma reactor but not on the surface of the BaTiO<sub>3</sub>-packed reactor. Although packing BaTiO<sub>3</sub> in the plasma reactor reduced the onset voltage, it did not promote the propagation of plasma on the surface.

The porosity of the different materials also played a role in their performance in the pyrolysis–plasma/catalysis of the waste plastic. MCM-41 has the highest porosity among the materials tested; the high porosity enhances the plasma discharge by generation of plasma within the pores in addition to the microdischarges between particles and surface discharges on the surface. Zhang et al.<sup>50</sup> theoretically investigated the generation of plasma inside catalyst pores of materials with different dielectric constants ranging from 4 to 1000. They found that there was an enhanced ionization in the pores of materials with a low dielectric constant (<200), while for high-dielectric-constant materials (>1000), there was negligible ionization in the pores due to polarization of both sidewalls resulting in a reduced electric field. They concluded that common catalyst supports with dielectric constants between 4 and 11 allow microdischarges to be easily formed inside the catalyst pores even for smaller pore sizes. The work of Zhang et al.<sup>50</sup> involved pore sizes of 10–50 μm, significantly larger than found for the materials in this work. However, in a later paper by the same group,<sup>51</sup> it was reported that plasma discharge streamers could penetrate into the surface features of porous catalysts with the formation of microdischarges inside nanometer-sized pores as well as micrometer-sized pores. The ionization takes place mainly near or inside the pores and leads to a high electron density. The maximum electric field and electron density were found for pore sizes between 4 and 10 nm. Their modeling showed that enhanced microdischarges could form near and inside the pores of mesoporous catalysts, i.e., similar in the pore size range to the materials used in our work. It has also been reported<sup>52,53</sup> that the plasma/catalyst environment involving reactive gases can form plasma discharge streamers possessing high electron densities and

thereby may be able to penetrate nanometer-sized catalyst pores. Such a highly reactive suite of gases would be formed from the pyrolysis of the waste plastic HDPE, including hydrogen, methane, C<sub>2</sub>–C<sub>4</sub> hydrocarbon gases, and a wide range of higher-molecular-weight *n*-alkanes and lower concentrations of alkenes and alkadienes.<sup>14</sup> The different performances by the different zeolites also suggested that the composition of the materials is not as important as the porosity since MCM-41, Y-zeolite, and ZSM-5 are all aluminosilicates and have similar dielectric constants but gave different performances in terms of hydrogen production. It therefore may be concluded that the difference in the surface area and porosity affected the performance of the different materials in this work. The use of porous materials in the discharge zone has been reported to result in an enhanced performance of a DBD compared to when nonporous materials are used.<sup>54</sup>

Although discussion here, of the hydrogen yield and the different catalyst properties, has centered around the surface area, porosity, and dielectric properties of the catalysts, other catalytic properties should be considered. For example, altering the surface chemistry of the catalyst material to increase the acidity and basicity has been shown to influence the production of hydrogen,<sup>19,55</sup> for example, using zeolites for the production of hydrogen from pyrolysis–catalytic steam reforming of waste plastics<sup>19</sup> and metal oxide catalysts for the catalytic steam reforming of methane to produce hydrogen.<sup>55</sup> The catalyst preparation methods such as coprecipitation, impregnation, and sol–gel have also been shown to influence the properties of the catalyst such as the surface area, porosity, and metal particle size and metal particle dispersion, which in turn can affect the yield of hydrogen from the pyrolysis–catalytic steam reforming of waste plastics.<sup>56</sup> Such factors have not been investigated here but may have a higher impact on hydrogen production in the particular reaction environment of plasma/catalysis and require further investigation.

Among the nine catalyst materials studied, MCM-41 has the lowest bulk density, and as such, a higher volume of MCM-41 was used in the discharge zone compared to the other catalyst support materials since 1.0 g of support materials was loaded into the plasma/catalysis reactor in each case. To determine the effect of the material packing volume of the different support materials, experiments were undertaken using the same catalyst bed depth (material volume), irrespective of the mass used. Selected materials were used for the plasma/catalysis with the same volume of material equivalent to 1.0 g of MCM-41. The mass of BaTiO<sub>3</sub> was 4.7 g, CaTiO<sub>3</sub> was 3.0 g, and dolomite was 3.55 g, which gave the same catalyst support bed depth as 1.0 g of MCM-41. Figure 6 shows the gas composition from the pyrolysis–nonthermal plasma/catalysis of waste HDPE when the same volume of MCM-41, dolomite, BaTiO<sub>3</sub>, and CaTiO<sub>3</sub> was loaded in the plasma discharge zone. The results confirmed that different materials interact with the plasma in different ways. When a greater catalyst bed depth of dolomite was used, an enhanced hydrogen yield of 10 mmol g<sup>-1</sup><sub>plastic</sub> was obtained. This suggests that the increased contact area of the plasma and the higher volume and mass of the support material improved the plasma/catalyst reaction performance. In the case of BaTiO<sub>3</sub> and CaTiO<sub>3</sub>, the effect of the bed depth was negligible and may have been nullified by the high dielectric constant of the materials, which hampered the propagation of surface plasma discharge streamers on the material surfaces. In plasma/catalysis, surface streamers are

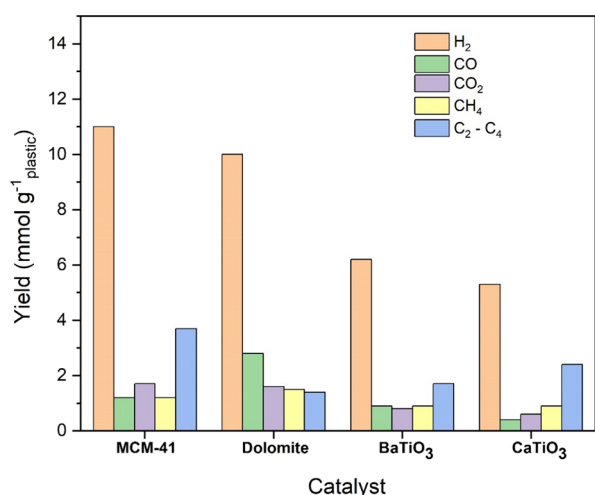


**Figure 6.** Gas composition from pyrolysis–nonthermal plasma/catalytic reforming of waste plastic using the same bed depth of catalyst support packing materials.

strongly related to the catalytic activity of the catalyst.<sup>57</sup> This result further confirmed that the MCM-41 was more active in the plasma/catalysis of the waste plastic pyrolysis volatiles among the packing materials investigated in this study.

**3.2.2. Influence of the Catalyst Support Material Particle Size.** The effect of the particle size of the catalyst support material on the hydrogen yield from the pyrolysis nonthermal plasma/catalytic reforming of waste plastic was investigated using the MCM-41 support material. The experiments were carried out by loading 1.0 g of different sizes of the MCM-41 with particle sizes of 50–212, 300–600, and 600–1000  $\mu\text{m}$  in the discharge zone. The discharge was sustained at 80 W, and steam reforming was carried out with a steam input of 2 g h<sup>-1</sup> g<sup>-1</sup> plastic. The total gas yield and the gas composition are shown in Table 4 and Figure 7, respectively. The smallest particle size

**Table 4. Influence of Process Parameters on the Gas Yield Obtained from Pyrolysis-Plasma/Catalysis of Waste Plastic**

| influence of MCM-41 particle size       |                      |                       |                        |                                   |
|---|----------------------|-----------------------|------------------------|-----------------------------------|
| MCM-41 particle size                    | 50–212 $\mu\text{m}$ | 300–600 $\mu\text{m}$ | 600–1000 $\mu\text{m}$ |                                   |
| gas yield (wt %)                        | 29.2                 | 13.8                  | 12.3                   |                                   |
| influence of the catalyst:plastic ratio |                      |                       |                        |                                   |
| catalyst:plastic ratio                  | 1:1                  | 3:4                   | 1:2                    | 1:4                               |
| gas yield (wt %)                        | 29.2                 | 20.1                  | 16.6                   | 13.4                              |
| influence of nickel impregnation        |                      |                       |                        |                                   |
| Ni catalyst support                     | Ni/MCM-41            | Ni/Y-zeolite          | Ni/BaTiO <sub>3</sub>  | Ni/Al <sub>2</sub> O <sub>3</sub> |
| gas yield (wt %)                        | 33.3                 | 29.1                  | 9.5                    | 20.3                              |

of 50–212  $\mu\text{m}$  showed the highest performance in terms of the total gas yield. A gas yield of 29.2 wt % was obtained compared to 13.8 and 12.3 wt % obtained with particle sizes of 300–600 and 600–1000  $\mu\text{m}$ , respectively. This shows that the smallest particle size was more active in cracking the tar to produce gases. Figure 7 shows that there was a significant difference in the performance of different particle sizes of MCM-41. An increase in the hydrogen yield was obtained with a decrease in the particle sizes; for example, 11 mmol g<sup>-1</sup> of hydrogen was obtained with the smallest MCM-41 particle size of 50–212  $\mu\text{m}$ . When the particle size was increased to 300–600  $\mu\text{m}$ , the

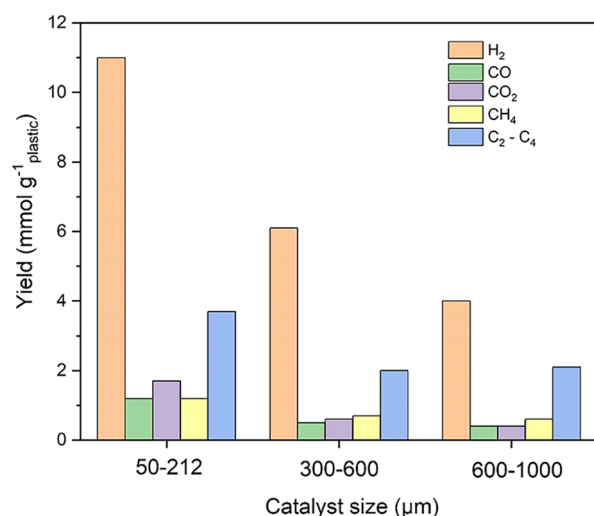


**Figure 7.** Gas composition from pyrolysis–nonthermal plasma reforming of HDPE using different particle sizes of MCM-41.

hydrogen yield decreased to 6.1 mmol g<sup>-1</sup>, and when a particle size of 600–1000  $\mu\text{m}$  was used, a hydrogen yield of 4 mmol g<sup>-1</sup> was obtained. Similar trends were observed for the yields of CO, CO<sub>2</sub>, CH<sub>4</sub>, and the light hydrocarbons.

Two types of discharges exist in a plasma/catalysis reactor, namely, partial discharge, which is the discharge that occurs at the contact points of the catalyst support material, and surface streamers, which are discharges on the surface of the material. The smaller the particle size, the higher the contact points between a particle and a particle, a particle and the electrode, and a particle and the dielectric barrier, where partial discharges can be generated. These partial discharges augment the electric field inside the reactor resulting in more decomposition of the pyrolysis volatile hydrocarbons into lower-molecular-weight hydrocarbons. The smaller sized particles also had a more available surface where more plasma discharge streamers are produced that propagate along the catalyst surface, thereby increasing the discharge area. The reduced void space in the reactor when small particles were used increased the residence time of the reactant gases with the support material resulting in more cracking and reaction of the reactants to produce syngas. These observations are in agreement with the work of Patil et al.<sup>48</sup> who observed the most effective performance of the catalyst with a particle size of 250–160  $\mu\text{m}$  among the different ranges of catalyst particle sizes investigated for plasma/catalytic NO<sub>x</sub> synthesis. Bogaerts et al.<sup>53</sup> modeled the behavior of the discharge in a plasma/catalysis environment and observed an enhancement of the electric field when smaller-particle-size beads were used compared to larger sized beads due to the higher number of available contact points.

**3.2.3. Influence of the Catalyst:Plastic Ratio.** Further work was carried out with the MCM-41 to investigate the effect of the bed depth on nonthermal plasma/catalysis. The experiments were conducted by placing different masses of MCM-41 (0.25, 0.50, 0.75, and 1.0 g) in the DBD reactor, representing catalyst:plastic ratios of 1:4, 1:2, 3:4, and 1:1. For all the experiments, the discharge was sustained at a power input of 80 W, and the reactor was maintained at 250 °C. The results of the gas yield obtained using the different masses of the MCM-41 are shown in Table 4. Varying the mass of the MCM-41 means that a different catalyst bed depth is obtained since the

same reactor was used in each case. Table 4 shows the variation of the total gas yield obtained from different catalyst bed depths. Increasing the mass of the MCM-41 resulted in an increase in the total gas yield. The highest gas yield of 29.2 wt % was obtained when the catalyst:plastic ratio was 1:1, representing the highest mass of the MCM-41. Reducing the mass of MCM-41 in the discharge zone produced a marked reduction in total gas yield to only 13.4 wt %, obtained with the lowest mass of MCM-41 studied at a catalyst:plastic ratio of 1:4.

Figure 8 shows the gas composition obtained when different weights of MCM-41 were used in the discharge zone. An

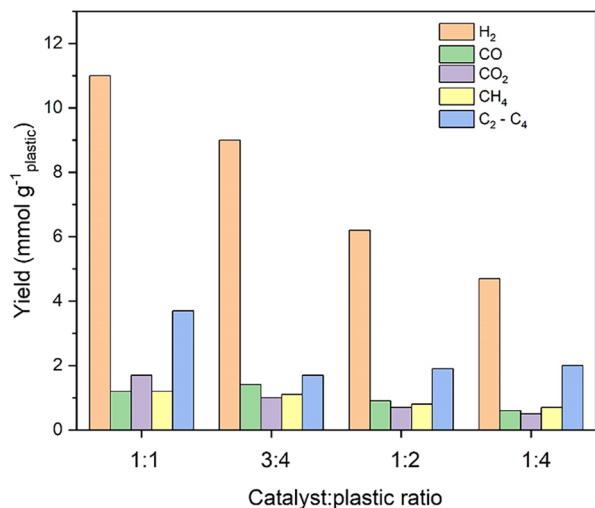


**Figure 8.** Gas composition from pyrolysis–nonthermal plasma reforming of HDPE using different catalyst:plastic ratios.

approximately linear relationship exists between the catalyst weight and its performance in terms of the hydrogen yield. The hydrogen yield increased with an increase in the catalyst weight. For example, the hydrogen yield was 11 mmol g<sup>-1</sup> plastic when the catalyst:plastic ratio of 1:1 was used. The hydrogen yield then reduced to 9, to 6.2, and then to 4.7 mmol g<sup>-1</sup> plastic when the mass of MCM-41 was reduced in relation to the plastic feedstock, at catalyst:plastic ratios of 3:4, 1:2, and 1:4, respectively. The yields of CO, CO<sub>2</sub>, CH<sub>4</sub>, and the light hydrocarbons also followed this trend. A higher contact area between the catalyst and the plasma resulted in a stronger interaction. As the bed depth was increased due to the change in mass of the catalyst, the area of contact between the discharge plasma and the catalyst would also increase.

**3.2.4. Influence of Nickel Impregnation of the Support Materials.** In conventional catalytic steam reforming reactions, nickel-based catalysts are known for their excellent catalytic activity. To study the influence of nickel-supported catalysts on the pyrolysis–plasma/catalysis of waste plastics, nickel-supported catalysts (10 wt %) were prepared using the support materials MCM-41, Y-zeolite, BaTiO<sub>3</sub>, and Ni/Al<sub>2</sub>O<sub>3</sub>. In each case, 1.0 g of the Ni-supported catalyst of 50–212 μm catalyst particle size was loaded in the discharge zone of the plasma reactor, and the plasma discharge was sustained at 80 W. Steam reforming of the waste plastic-derived pyrolysis volatiles took place with a steam flow rate of 2 g h<sup>-1</sup>. Table 4 shows the total gas yield obtained when the four different nickel-supported catalysts were used in the pyrolysis–plasma/catalysis reactor system. The presence of nickel-supported

catalysts enhanced the catalytic properties of the materials, which gave higher yields of total gas and hydrogen for the Ni/MCM-41, Ni/Y-zeolite, and Ni/Al<sub>2</sub>O<sub>3</sub> catalysts, but showed a decrease for the Ni/BaTiO<sub>3</sub> catalyst. As shown in Table 4, the highest total gas yield achieved with the Ni-based catalysts was 33.3 wt % obtained with the Ni/MCM-41 catalyst compared with 29.6 wt % for MCM-41 alone. For Ni/Y-zeolite, the gas yield increased to 29.1 when Ni was impregnated on Y-zeolite compared to 26.7 wt % with Y-zeolite alone. In the case of Al<sub>2</sub>O<sub>3</sub>, the gas yield increased from 16.5 to 20.3 wt % when Ni/Al<sub>2</sub>O<sub>3</sub> was used. On the other hand, a decrease in the gas yield from 12.7 to 9.5 wt % was observed when Ni on barium titanate was used compared to BaTiO<sub>3</sub> alone.

The composition of the product gas from the pyrolysis–plasma/catalysis of the waste plastics in relation to the Ni-based materials is illustrated in Figure 9. The results show that

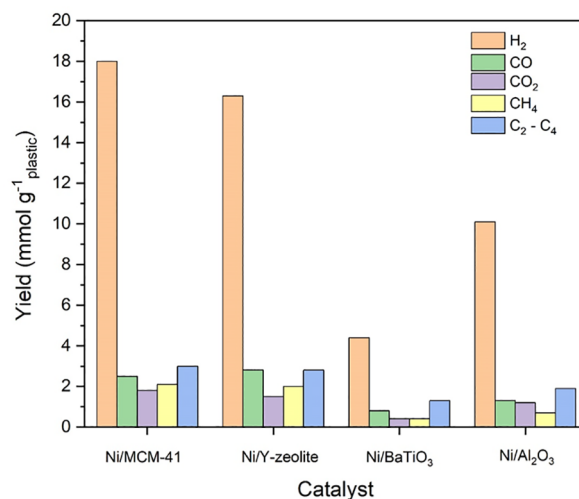


**Figure 9.** Gas composition from pyrolysis–nonthermal plasma reforming of HDPE using different nickel-based catalysts.

the presence of nickel on the MCM-41, Y-zeolite, and Al<sub>2</sub>O<sub>3</sub> improved the performance in terms of hydrogen production compared to when the support materials alone were used. The highest H<sub>2</sub> yield of 18 mmol g<sup>-1</sup> plastic and a CO yield of 2.5 mmol g<sup>-1</sup> plastic were obtained with Ni/MCM-41. This is attributed to the role of nickel in the interaction of plasma, reactants, and support materials. The presence of a metal on the support allows charge accumulation on the catalyst surface, thereby improving the charge transfer between electrodes.<sup>58</sup> The increase in the hydrogen selectivity can also be attributed to the dehydrogenation of the light hydrocarbons over the nickel particles caused by plasma-induced gaseous reactions.<sup>25</sup>

Other researchers working on plasma/catalysis have reported improved performance of the catalyst especially with regard to reactivity and selectivity when an active metal is impregnated on the catalyst material. For example, Kim and Ogata<sup>49</sup> packed zeolite pellets in a discharge barrier reactor and observed an enhancement of the plasma on the surface of the catalyst. Without the metal loading, the plasma was confined in the vicinity of the zeolite pellets, but when Ag-supported zeolites were used, the discharge became stronger and propagated on the surface of the catalyst. They concluded that the Ag nanoparticles helped the surface discharge streamers to be expanded over a larger area resulting in enhanced plasma/catalysis reactions. In the case of Ni/

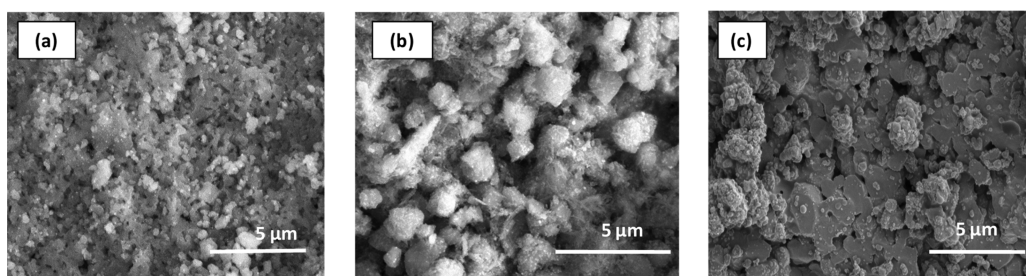


**Figure 10.** SEM images showing the surface morphology of the catalyst support materials (a) Ni/MCM-41, (b) Ni/Y-zeolite, and (c) Ni/BaTiO<sub>3</sub>.

BaTiO<sub>3</sub>, a reduced activity was observed when nickel was impregnated on the BaTiO<sub>3</sub> support compared to the BaTiO<sub>3</sub> material alone. The interaction of the impregnated nickel metal and the support may have prevented the propagation of surface discharge streamers, which resulted in a reduced performance of the catalyst in the plasma/catalysis system. Jo et al.<sup>59</sup> made a similar observation when they compared the degree of methane conversion in a DBD plasma reactor with Al<sub>2</sub>O<sub>3</sub> to that with a Pt-supported Al<sub>2</sub>O<sub>3</sub> catalyst. The Pt/Al<sub>2</sub>O<sub>3</sub> catalyst gave a lower methane conversion, which was attributed to a reduced electric field in the DBD plasma when Pt/Al<sub>2</sub>O<sub>3</sub> was loaded compared to when Al<sub>2</sub>O<sub>3</sub> alone was loaded.

Apart from the plasma/catalyst interaction, the catalytic effects provided by the chemical properties of the catalysts themselves play important roles in the plasma/catalyst environment. The catalyst is composed of the active metal and the support, and their interaction determines the catalytic activity and durability. The chemical species generated during the interaction between the plasma and the pyrolysis-derived hydrocarbon volatiles can react on the surface of the catalyst where the properties of the catalyst affect the surface reactions. Temperature-programmed reduction (TPR) of the prepared Ni-supported catalysts (Figure 4) showed that the Ni/MCM-41, Ni/Y-zeolite, and Ni/Al<sub>2</sub>O<sub>3</sub> catalysts have a strong metal–support interaction, whereas the Ni/BaTiO<sub>3</sub> catalyst has a weak metal–support interaction. Alayat et al.<sup>60</sup> reported that catalysts with strong metal–support interactions show a higher surface dispersion of metal particles, which lead to a small particle size of the metal and a higher supported metal dispersion. On the other hand, a weak metal–support interaction leads to a low metal dispersion, which results in agglomeration of the metal.

Three of the nickel-based catalysts, Ni/MCM-41, Ni/Y-zeolite, and Ni/BaTiO<sub>3</sub>, were examined for their surface morphology using scanning electron microscopy (SEM). Figure 10 shows the SEM images of the surfaces of the three catalysts. Clearly, nickel particles were well dispersed over the surfaces of the Ni/MCM-41 and the Ni/Y-zeolite catalysts. This increased the active sites for the steam reforming reactions. The uniform and dispersed nickel particles also imply that the materials are porous, and they have a strong metal–support interaction as shown by the results of the TPR. The SEM image of the Ni/BaTiO<sub>3</sub> shows large nonuniform nickel particles over the BaTiO<sub>3</sub> surface that indicate agglomeration of the impregnated nickel on the surface. To obtain more information on the porosity and nickel distribution inside the catalyst, FIB-SEM was used to obtain cross-sectional images of the catalyst and also EDX nickel mapping of nickel throughout the catalyst particles. The FIB-SEM and EDX mapping results are shown in Figure 11. The FIB-SEM

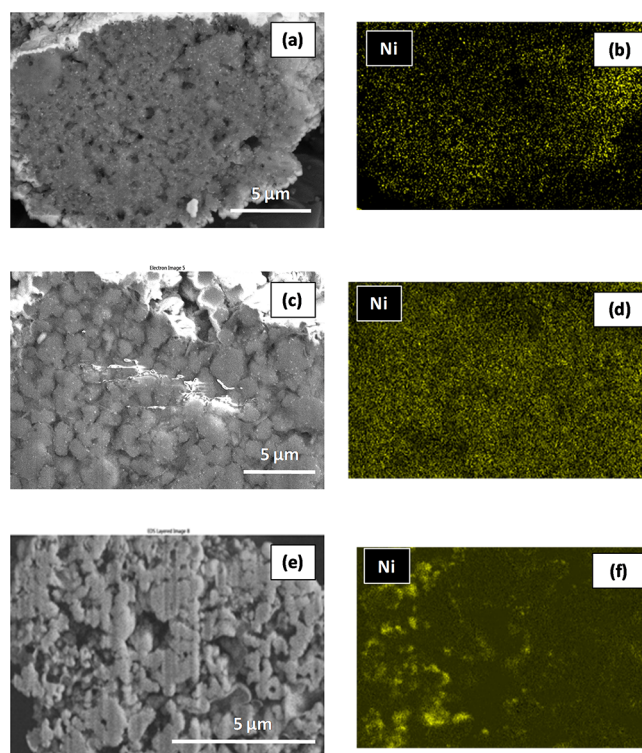


**Figure 11.** FIB-SEM cross-sectional images of (a) Ni/MCM-41, (c) Ni/Y-zeolite, and (e) Ni/BaTiO<sub>3</sub>; (b) EDX nickel mapping of Ni/MCM-41, (d) Ni/Y-zeolite, and (f) Ni/BaTiO<sub>3</sub>.

images (Figure 11a, c, and e) of the cross section showed a loose structure of the Ni/MCM-41 and Ni/Y-zeolite catalysts, which confirmed their porosity. Nickel was well dispersed over the cross section of the catalysts, and this can be seen more clearly from the EDX nickel mapping (Figure 11b, d, and f). For the Ni/BaTiO<sub>3</sub>, the image of the cross section did not show nickel distribution inside the catalyst but rather on the surface. The EDX nickel mapping of the cross section showed nickel enrichment near the surface of the catalyst but not inside. It is suggested that the nickel particles on the Ni/MCM-41 and Ni/Y-zeolite catalysts were smaller and well dispersed and penetrated the pores of the materials where more chemical reactions could occur. The particle agglomeration in the case of Ni/BaTiO<sub>3</sub> prevented the penetration of the nickel particles inside the catalyst as indicated earlier; additionally, the smaller pore diameter and the low pore volume may also have restricted access of the nickel to the catalyst pores.

**3.2.5. Plasma/Catalysis Synergy Compared to Plasma and Catalysis.** The influence of the synergistic interaction between plasma and the catalyst in relation to the pyrolysis–

plasma/catalysis of waste plastic in terms of total gas yield and hydrogen production was investigated. Experiments to investigate the significance of the synergy between plasma and the catalyst were carried out: (i) with plasma alone at 80 W without a catalyst, (ii) with a 10 wt % Ni/MCM-41 catalyst at a low temperature (250 °C) in the absence of plasma, and (iii) a combination of plasma/catalysis with the plasma sustained at 80 W and with the 10 wt % Ni/MCM-41 catalyst. All the experiments were carried out with a steam flow rate of 2 g h<sup>-1</sup>. Table 5 compares the total gas yield obtained from these experiments.

**Table 5. Comparison of the Total Gas Yield from Catalysis, Plasma Alone, and Plasma/Catalysis of the Pyrolysis Vapors of Waste HDPE (10 wt % Ni/Al<sub>2</sub>O<sub>3</sub> Catalyst)**

|                  | catalyst only | plasma only | plasma/catalysis |
|------------------|---------------|-------------|------------------|
| gas yield (wt %) | 8.1           | 15.0        | 33.3             |

When the MCM-41 was used alone, the total gas yield was 8.1 wt %. Thermal catalytic reforming with Ni-based catalysts typically uses catalyst temperatures of ~800 °C; however, at a low temperature of 250 °C, the catalyst temperature used in this work, the catalyst was not activated, and there appeared to be no further cracking or reforming of the pyrolysis gases in the second-stage catalyst reactor. With the introduction of the plasma processing (no catalyst), a total gas yield of 15.0 wt % was obtained, which suggested that the plasma was able to crack some of the derived plastic pyrolysis gases. The combination of plasma and the catalyst showed a synergy because a gas yield of 33.3 wt % was obtained, which was significantly higher than that obtained by the catalyst only and plasma only.

Figure 12 shows the composition of the gases obtained from the experiments. A low hydrogen yield of only 0.1 mmol

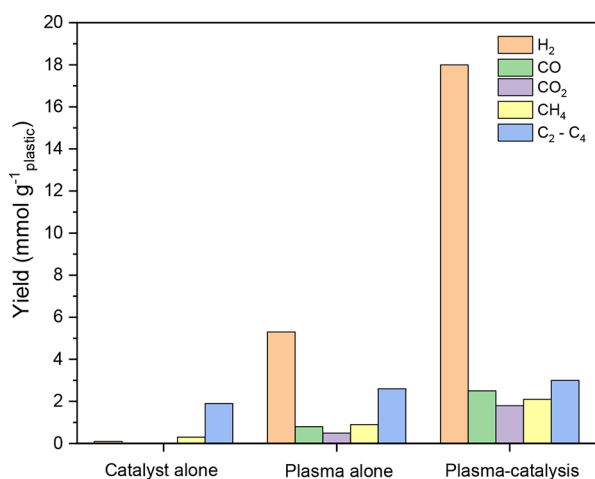


**Figure 12.** Comparison of the gas composition from catalysis, plasma alone, and plasma/catalysis of the pyrolysis vapors of waste HDPE.

g<sup>-1</sup> plastic and no formation of carbon oxides were obtained when the MCM-41 alone was used, implying that no further cracking of the pyrolysis gases or steam reforming occurred in the second-stage reactor at the catalyst process temperature of 250 °C. The product gases comprised CH<sub>4</sub> and also C<sub>2</sub>-C<sub>4</sub> hydrocarbons with a yield of 1.9 mmol g<sup>-1</sup> plastic.

Using plasma alone (no catalyst) at 80 W for the steam reforming of the plastic pyrolysis gases produced 5.3 mmol g<sup>-1</sup> plastic of hydrogen and 0.8 mmol g<sup>-1</sup> plastic of CO, suggesting that catalytic steam reforming of the pyrolysis gases was taking place. In addition, 0.9 mmol g<sup>-1</sup> plastic of CH<sub>4</sub> and 2.6 mmol g<sup>-1</sup> plastic of C<sub>2</sub>-C<sub>4</sub> hydrocarbons were produced. In the absence of any catalyst or support material, packing in the discharge zone of the reactor prevents any formation of filamentary microdischarges that are generated over the dielectric surface of the support packing material and extending across the discharge gap between the electrodes of the plasma reactor.<sup>44</sup> However, the presence of the plasma generated reactive radicals from the interaction of the pyrolysis gases and the plasma producing various reactions in the gas phase to produce syngas and light hydrocarbons. Other researchers have reported similar findings for plasma-gas interactions.<sup>61,62</sup>

For the plasma/catalytic steam reforming of the plastic pyrolysis gases, with the plasma maintained at 80 W and in the presence of the 10 wt % Ni-MCM-41 catalyst, the total gas yield was markedly increased to 33.3 wt %. It is clear that catalytic steam reforming of the pyrolysis hydrocarbon gases occurred resulting in the production of 18 mmol g<sup>-1</sup> plastic of hydrogen and 2.5 mmol g<sup>-1</sup> plastic of CO. In addition, the yield of the other gases was also higher than in the case of the catalyst alone or plasma alone, with the production of 1.8 mmol g<sup>-1</sup> plastic of CO<sub>2</sub>, 2.1 mmol g<sup>-1</sup> plastic of CH<sub>4</sub>, and 3 mmol g<sup>-1</sup> plastic of C<sub>2</sub>-C<sub>4</sub> hydrocarbons. This indicates that at the low experimental temperature used of 250 °C, the conversion of the pyrolysis gases into syngas and other hydrocarbons took place via plasma-induced catalytic reactions. Clearly, the interaction of the plasma and the catalyst has produced a synergy, which is greater than what was produced in the plasma alone or catalysis alone reaction environments. The catalyst was only effectively activated in the presence of the plasma, and the pyrolysis hydrocarbons were steam reformed in the presence of the catalyst. The plasma/catalysis enhanced both the yield and selectivity of the gaseous products. In the case of the plasma/catalysis, the plasma served as the heat, electron, and radical source.<sup>63</sup> Synergy in plasma/catalysis has also been reported by other researchers.<sup>64,65</sup> For example, Zhang et al.<sup>66</sup> demonstrated a synergy in the plasma/catalytic dry reforming of methane using different Cu-Ni/γ-Al<sub>2</sub>O<sub>3</sub> catalysts. They attributed this to surface adsorption of reactive plasma species followed by the recombination of the adsorbed species.

The mechanism of the synergy effect may be suggested in that the plasma-catalyst combination affects the conversion in two possible ways. First, the plasma and the catalyst can separately affect the gas conversion by inducing plasma chemical reactions and by lowering the activation barrier of the process, respectively. Second, the mutual interaction of the plasma and the catalyst can affect the process. The roughness and porosity of the catalyst can enhance the electric field, which directly affects the electron density distribution function and thus the electron impact dissociation and ionization rates. The discharge is also changed from filamentary to a mixture of surface discharges, which leads to increased electron impact reaction rates. The reactants can also be adsorbed on the catalyst surface resulting in a longer retention time in the reactor and therefore increased conversion of the volatiles. On the other hand, the plasma can affect the physicochemical properties of the catalyst by increasing the adsorption probability and the total surface area of the catalyst. In

addition, the formation of strong microdischarges can result in the formation of hot spots, which can locally activate the catalyst thermally. In addition, one of the advantages of the plasma/catalytic process is that it operates at a low temperature, for example, at 250 °C in this work. However, although, the overall temperature of the DBD plasma/catalyst reactor was 250 °C, the interaction of the plasma and the catalyst can generate local high-temperature hot spots due to microdischarges.<sup>52</sup> Therefore, the higher temperatures required for efficient thermal catalytic steam reforming may be achieved in local regions of the plasma/catalyst surface and pores.

**3.2.6. Stability of the 10 wt % Ni/MCM-41 Catalyst.** Maintaining the activity and stability of the catalyst during the pyrolysis–plasma/catalysis process is important for the development of the process. The most effective catalyst for the production of total gas, syngas, and hydrogen was the 10 wt % Ni/MCM-41 catalyst and was subjected to a catalyst stability test over six experiments. The experiment was carried out by using the same catalyst under plasma/catalyst conditions, with the same catalyst in the discharge zone and replenishing the plastic feedstock plastic for each of the six experiments. Thereby, a total catalyst time on-stream of 3 h was used. The plasma was sustained at 80 W, and a steam flow rate of 2 g h<sup>-1</sup> was used. Figure 13 shows the gas composition

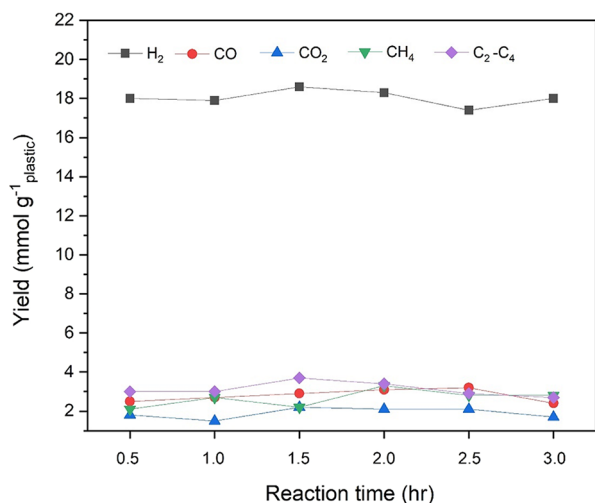


**Figure 13.** Gas composition from pyrolysis–catalysis of waste HDPE using the same Ni/MCM-41 catalyst for 3 h.

during the 3 h experiment. It can be seen from the figure that a quite stable yield of all the gases was obtained over the 3 h catalyst on-stream period, implying that the catalyst was stable and active for the duration of the process, albeit a relatively short period of testing.

The pyrolysis–plasma/catalytic steam reforming of waste plastic (HDPE) with the different support materials showed that the highest hydrogen yield achieved was 11 mmol g<sup>-1</sup> plastic with the MCM-41 material. When nickel was added to the different materials, the highest hydrogen yield was produced with the 10 wt % Ni-MCM-41 catalyst at 18 mmol g<sup>-1</sup> plastic. The yield of hydrogen is disappointingly low compared with reported yields of hydrogen from the nonplasma processing of waste plastics using conventional pyrolysis–catalytic steam reforming. For example, fluidized-bed pyrolysis–catalytic steam reforming of polypropylene produced a hydrogen yield

of 168 mmol g<sup>-1</sup> plastic<sup>21</sup> and two-stage spouted-bed fluidized-bed pyrolysis with fluidized-bed catalytic steam reforming produced a hydrogen yield of 185 mmol g<sup>-1</sup> plastic from polyethylene.<sup>22</sup> The advantage of these examples was that they were a continuous operation, which carries the potential for ease of scaling up. Meanwhile, the pyrolysis–plasma/catalytic steam reforming of plastics described in our work used fixed-bed reactors. Scaling-up the reactor system is the key to the development of the process, which is difficult for plasma/catalysis processes due to the low economies of scale.<sup>67</sup> Indeed, in a recent “roadmap” for the development of plasma/catalysis technologies, it has been suggested that it is unrealistic to expect plasma/catalytic processes to be scaled up to compete with large-scale thermal catalytic processes, such as that used for the commercial production of hydrogen from natural gas by catalytic steam reforming.<sup>67</sup> Rather, it is proposed that the role of plasma/catalysis is better suited to small-scale units operating in niche areas.<sup>67</sup> The small-scale pyrolysis–plasma/catalysis of waste plastics may therefore have a role to play in the future sustainable management of waste plastics but for localized areas, where the waste plastics are generated, collected, and treated locally. That scenario presupposes that the process can be developed to ensure that higher yields of hydrogen are produced since it should be emphasized that the advantage of the plasma/catalysis process is the low overall operating temperature of the plasma/catalyst reforming reactor at 250 °C compared to thermal catalytic reforming at ~800 °C. In addition, the plasma technology is reported to have low investment and operating costs and can be supplied on a modular basis for distributed use.<sup>67</sup>

#### 4. CONCLUSIONS

Nine different substrates were tested for their activity in the pyrolysis–plasma/catalytic steam reforming of waste plastic (HDPE) pyrolysis gases. Despite the similar reaction conditions, different packing materials performed differently in terms of the gas yield and composition, indicating the important role played by the catalyst in the plasma/catalysis process. Among the tested materials, MCM-41 gave the best performance with a gas yield of 29.2 wt % and a hydrogen yield of 11 mmol g<sup>-1</sup> plastic. The different properties of the materials such as the BET surface area, the BJH pore volume, and the dielectric constant affected the plasma/catalyst interactions and their activities in the reactions. The influence of particle size on the yield of total gas, syngas, and hydrogen was investigated using different sizes of the MCM-41, and the smallest particle size gave the highest yield of hydrogen. Increasing the amount of the catalyst in the discharge zone (increasing the catalyst:plastic ratio) increased the yield of total gas, syngas, and hydrogen. Nickel was impregnated on some selected support materials and the catalysts used for pyrolysis–plasma/catalysis. The performance was enhanced in the case of Ni/MCM-41 and Ni/Y-zeolite catalysts, but no improvement in the catalytic activity was observed in the case of Ni/BaTiO<sub>3</sub>. The 10 wt % MCM-41 catalysts produced the highest hydrogen yield of 18 mmol g<sup>-1</sup> plastic. The Ni/MCM-41 and Ni/Y-zeolite enhanced the hydrogen production from the pyrolysis–plasma/catalysis of the plastic, which was linked to their low dielectric constant and the high surface area and porosity, which affected their discharge properties and thereby their catalytic activity. A catalyst stability test carried out with the Ni/MCM-41 for 3 h revealed a stable yield of all the gases, which indicates the catalyst’s stability and activity after 3 h of

catalyst on-stream. This study shows that different catalyst support/packing materials have different effects on the plasma-induced discharge in the plasma/catalysis reaction environment. Among the catalyst support materials tested in this study, the materials with a high surface area and porosity and a low dielectric constant showed a better improvement of the discharge and consequently enhancement of the catalytic activity for the catalytic steam reforming of waste plastic. Furthermore, synergy of the plasma/catalysis system depends on the properties of the support packing materials used in the discharge zone. However, other factors such as the surface chemistry of the materials used in the plasma/catalyst zone should be considered as influencing factors on material performance in relation to hydrogen yield, for example, the surface chemistry, acidity and basicity of the material, the dispersion and particle size of the active metal on the catalyst surface and within pores, the use of metal promoters to enhance hydrogen yield, etc. Such factors may in fact have a more significant impact on hydrogen yield for the development of the pyrolysis–plasma/catalytic processing of waste plastics for production of hydrogen.

## AUTHOR INFORMATION

### Corresponding Author

Paul T. Williams – School of Chemical & Process Engineering,  
University of Leeds, Leeds LS2 9JT, United Kingdom;  
orcid.org/0000-0003-0401-9326; Phone: 44  
1133432504; Email: p.t.williams@leeds.ac.uk

### Authors

Idris Aminu – School of Chemical & Process Engineering,  
University of Leeds, Leeds LS2 9JT, United Kingdom  
Mohamad A. Nahil – School of Chemical & Process  
Engineering, University of Leeds, Leeds LS2 9JT, United  
Kingdom

Complete contact information is available at:  
<https://pubs.acs.org/10.1021/acs.energyfuels.1c04186>

### Notes

The authors declare no competing financial interest.

## REFERENCES

- (1) PlasticsEurope Plastics-the facts 2020. *PlasticsEurope*; 2020.
- (2) Geyer, R.; Jambeck, J. R.; Law, K. L. Production, use, and fate of all plastics ever made. *Sci. Adv.* **2017**, *3*, No. e1700782.
- (3) Jambeck, J. R.; Geyer, R.; Wicox, C.; Siegler, T. R.; Perryman, M.; Andrady, A.; Narayan, R.; Law, K. L. Plastic waste inputs from land into the ocean. *Science* **2015**, *347*, 768–771.
- (4) European Commission A *European Strategy for Plastics in a Circular Economy*; European Commission: Brussels: Belgium, 2018.
- (5) Hydrogen Council *Hydrogen scaling up: A sustainable pathway for the global energy transition*; Hydrogen Council: 2017
- (6) Gutiérrez-Martín, F.; Amodio, L.; Pagano, M. Hydrogen production by water electrolysis and off-grid solar PV. *Int. J. Hydrogen Energy* **2021**, *46*, 29038–29048.
- (7) Vertes, A. A.; Qureshi, N.; Blaschek, H. P.; Yukawa, H. *Green Energy to Sustainability: Strategies for Global Industries*; John Wiley & Sons Ltd: 2020, pp. 425–445.
- (8) Wang, J.; Yi, Y.; Wu, C.; Guo, H.; Tu, X. Enhanced hydrogen production from catalytic biomass gasification with in-situ CO<sub>2</sub> capture. *Environ. Pollut.* **2020**, *267*, 115487.
- (9) Zhang, Y.; Huang, J.; Williams, P. T. Fe–Ni–MCM-41 catalysts for hydrogen-rich syngas production from waste plastics by pyrolysis–catalytic steam reforming. *Energy Fuels* **2017**, *31*, 8497–8504.
- (10) Arregi, A.; Abadi, M. S. A.; Lopez, G.; Santamaria, L.; Artetxe, M.; Bilbao, J.; Olazar, M. CeO<sub>2</sub> and La<sub>2</sub>O<sub>3</sub> promoters in the steam reforming of polyolefinic waste plastic pyrolysis volatiles on Ni-based catalysts. *ACS Sustainable Chem. Eng.* **2020**, *8*, 17307–17321.
- (11) Chai, Y.; Gao, N.; Wang, M.; Wu, C. H<sub>2</sub> Production from co-pyrolysis/gasification of waste plastics and biomass under novel catalyst Ni–CaO–C. *Chem. Eng. J.* **2020**, *382*, 122947.
- (12) Barbarias, I.; Artetxe, M.; Lopez, G.; Arregi, A.; Santamaria, L.; Bilbao, J.; Olazar, M. Catalyst performance in the HDPE pyrolysis-reforming under reaction-regeneration cycles. *Catalysts* **2019**, *9*, 414.
- (13) Lopez, G.; Artetxe, M.; Amutio, M.; Alvarez, J.; Bilbao, J.; Olazar, M. Recent advances in the gasification of waste plastics. A critical overview. *Renewable and Sustainable Energy Reviews.* **2017**, *82*, 576–596.
- (14) Williams, P. T. Hydrogen and carbon nanotubes from pyrolysis-catalysis of waste plastics: A review. *Waste Biomass Valorization* **2021**, *12*, 1–28.
- (15) Aminu, I.; Nahil, M. A.; Williams, P. T. Hydrogen from waste plastics by two-stage pyrolysis/low-temperature plasma catalytic processing. *Energy Fuels* **2020**, *34*, 11679–11689.
- (16) Mei, D.; Tu, X. Atmospheric pressure non-thermal plasma activation of CO<sub>2</sub> in a packed-bed dielectric barrier discharge reactor. *ChemPhysChem* **2017**, *18*, 3253–3259.
- (17) Kim, H. H.; Terramoto, Y.; Ogata, A.; Takagi, H.; Nanba, T. Plasma catalysis for environmental treatment and energy applications. *Plasma Chem. Plasma Process.* **2016**, *36*, 45–72.
- (18) Wang, L.; Yi, Y.; Wu, C.; Guo, H.; Tu, X. One-step reforming of CO<sub>2</sub> and CH<sub>4</sub> to high-value liquid chemicals and fuels at room temperature by plasma-driven catalysis. *Angew. Chem. Int. Ed.* **2017**, *56*, 13679–13683.
- (19) Yao, D.; Yang, H.; Chen, H.; Williams, P. T. Investigation of nickel-impregnated zeolite catalysts for hydrogen/syngas production from the catalytic reforming of waste polyethylene. *Appl. Catal., B* **2018**, *227*, 477–487.
- (20) Wu, C.; Williams, P. T. Hydrogen from waste plastics by way of pyrolysis-gasification. *Waste and Resource Management: Waste Resour. Manage.* **2014**, *167*, 35–46.
- (21) Czernik, S.; French, R. Production of hydrogen from plastics by pyrolysis and catalytic steam reform. *Energy Fuels* **2006**, *20*, 754–758.
- (22) Barbarias, I.; Lopez, G.; Artetxe, M.; Arregi, A.; Santamaria, L.; Bilbao, J.; Olazar, M. Valorisation of different waste plastics by pyrolysis and in-line catalytic steam reforming for hydrogen production. *Energy Conversion Manage.* **2018**, *156*, 575–584.
- (23) Chen, H.; Mu, Y.; Shao, Y.; Chansai, S.; Xu, S.; Stere, C.; Xiang, H.; Zhang, R.; Yilai, J.; Fan, X.; Hardacre, C. Coupling non-thermal plasma with Ni catalysts supported on BETA zeolite for catalytic CO<sub>2</sub> methanation. *Catal. Sci. Technol.* **2019**, *9*, 4135–4145.
- (24) Wang, Y.; Craven, M.; Yu, X.; Ding, J.; Bryant, P.; Huang, J.; TU, X. Plasma-enhanced catalytic synthesis of ammonia over a Ni/Al<sub>2</sub>O<sub>3</sub> catalyst at near-room temperature: insights into the importance of the catalyst surface on the reaction mechanism. *ACS Catal.* **2019**, *9*, 10780–10793.
- (25) Zeng, Y. X.; Wang, L.; Wu, C.; Wang, J. Q.; Shen, X.; Tu, X. Low temperature reforming of biogas over K-, Mg- and Ce-promoted Ni/Al<sub>2</sub>O<sub>3</sub> catalysts for the production of hydrogen rich syngas: Understanding plasma-catalytic synergy. *Appl. Catal., B* **2018**, *224*, 469–478.
- (26) Mei, D.; Liu, S.; Tu, X. CO<sub>2</sub> reforming with methane for syngas production using a dielectric barrier discharge plasma coupled with Ni/γ-Al<sub>2</sub>O<sub>3</sub> catalysts: Process optimization through response surface methodology. *J. CO<sub>2</sub> Util.* **2017**, *21*, 314–326.
- (27) Wanke, S. E.; Flynn, P. C. The sintering of supported metal catalysts. *Catal. Rev. Sci. Eng.* **1975**, *12*, 93–135.
- (28) Grams, J.; Ruppert, A. Development of heterogeneous catalysts for thermo-chemical conversion of lignocellulosic biomass. *Energies* **2017**, *10*, 545.
- (29) Liu, B. S.; Au, C. T. Carbon deposition and catalyst stability over La<sub>2</sub>NiO<sub>4</sub>/γ-Al<sub>2</sub>O<sub>3</sub> during CO<sub>2</sub> reforming of methane to syngas. *Appl. Catal., A* **2003**, *244*, 181–195.

- (30) Azzolina-Jury, F.; Bento, D.; Henriques, C.; Thibault-Starzyk, F. Chemical engineering aspects of plasma-assisted CO<sub>2</sub> hydrogenation over nickel zeolites under partial vacuum. *J. CO<sub>2</sub> Util.* **2017**, *22*, 97–109.
- (31) Mei, D.; Ashford, B.; He, Y. L.; Tu, X. Plasma-catalytic reforming of biogas over supported Ni catalysts in a dielectric barrier discharge reactor: Effect of catalyst supports. *Plasma Processes Polym.* **2017**, *14*, 1600076.
- (32) Khoja, A.; Tahir, M.; Saidina Amin, N. A. Cold plasma dielectric barrier discharge reactor for dry reforming of methane over Ni/ $\gamma$ -Al<sub>2</sub>O<sub>3</sub>-MgO nanocomposite. *Fuel Process. Technol.* **2018**, *178*, 166–179.
- (33) Barbarias, I.; Lopez, G.; Artetxe, M.; Arregi, A.; Santamaria, L.; Bilbao, J.; Olazar, M. Pyrolysis and in-line catalytic steam reforming of polystyrene through a two-step reaction system. *J. Anal. Appl. Pyrolysis* **2016**, *122*, 502–510.
- (34) Fu, P.; Zhang, A.; Luo, S.; Yi, W.; Hu, S.; Zhang, Y. Catalytic steam reforming of biomass-derived acetic acid over two supported Ni catalysts for hydrogen-rich syngas production. *ACS Omega* **2019**, *4*, 13585–13593.
- (35) Yoshida, H.; Yamaoka, R.; Arai, M. Stable hydrogen production from ethanol through steam reforming reaction over nickel-containing smectite-derived catalyst. *Int. J. Mol. Sci.* **2015**, *16*, 350–362.
- (36) Wang, Y.; Wang, C.; Chen, M.; Tang, Z.; Yang, Z.; Hu, J.; Zhang, H. Hydrogen production from steam reforming ethanol over Ni/attapulgite catalysts - Part I: Effect of nickel content. *Fuel Process. Technol.* **2019**, *192*, 227–238.
- (37) Pelletier, L.; Liu, D. Stable nickel catalysts with alumina-aluminum phosphate supports for partial oxidation and carbon dioxide reforming of methane. *Appl. Catal., A* **2007**, *317*, 293–298.
- (38) Seo, J.; Youn, M.; Park, S.; Park, D.; Jung, J.; Chung, J. S.; Song, I. Hydrogen production by steam reforming of liquefied natural gas (LNG) over mesoporous nickel–alumina composite catalyst prepared by an anionic surfactant-templating method. *Catal. Today* **2009**, *146*, 44–49.
- (39) Sing, K. S. W. Reporting physisorption data for gas/solid systems with special reference to the determination of surface area and porosity (Recommendations 1984). *Pure Appl. Chem.* **1985**, *57*, 603–619.
- (40) Damyanova, S.; Pawelec, B.; Arishtirova, K.; Fierro, J. L. G.; Sener, C.; Dogu, T. MCM-41 supported PdNi catalysts for dry reforming of methane. *Appl. Catal., B* **2009**, *92*, 250–261.
- (41) Chen, J.; Yuanhua, Q.; Yongdan, L. Modification of Ni state to promote the stability of Ni-Al<sub>2</sub>O<sub>3</sub> catalyst in methane decomposition to produce hydrogen and carbon nanofibers. *J. Solid State Chem.* **2012**, *191*, 107–113.
- (42) Richardson, J.; Twigg, M. Reduction of impregnated NiO/ $\alpha$ -Al<sub>2</sub>O<sub>3</sub> association of Al<sup>3+</sup> ions with NiO. *Appl. Catal., A* **1998**, *167*, 57–64.
- (43) Williams, P. T.; Williams, E. Interaction of plastics in mixed plastics pyrolysis. *Energy Fuels* **1999**, *13*, 188–196.
- (44) Tu, X.; Gallon, H.; Twigg, M. V.; Gorry, P. A.; Whitehead, J. Dry reforming of methane over a Ni/Al<sub>2</sub>O<sub>3</sub> catalyst in a coaxial dielectric barrier discharge reactor. *J. Phys. D: Appl. Phys.* **2011**, *44*, 274007.
- (45) Fridman, A.; Kennedy, L., *Plasma Physics and Engineering*. 2011, Boca Raton, FL: CRC Press.
- (46) Ilic, J. *Wood: Electrical properties*, in Mahajan S. Encyclopedia of Materials: Science and Technology, Pergamon, Oxford, UK, 2001.
- (47) Rosenholtz, J. L.; Smith, D. T. The dielectric constant of mineral powders. *Am. Mineral.* **1936**, *21*, 115–120.
- (48) Patil, B. S.; Cherkasov, N.; Lang, J.; Ibhaddon, A. O.; Hessel, V.; Wang, Q. Low temperature plasma-catalytic NO<sub>x</sub> synthesis in a packed DBD reactor: Effect of support materials and supported active metal oxides. *Appl. Catal., B* **2016**, *194*, 123–133.
- (49) Kim, H. H.; Ogata, A. Nonthermal plasma activates catalyst: From current understanding and future prospects. *Eur. Phys. J. Appl. Phys.* **2011**, *55*, 13606.
- (50) Zhang, Y. R.; Neyts, E.; Bogaerts, A. Influence of the material dielectric constant on plasma generation inside catalyst Pores. *J. Phys. Chem. C* **2016**, *120*, 25923–25934.
- (51) Zhang, Y.; Wang, H. Y.; Zhang, Y. R.; Bogaerts, A. Formation of microdischarges inside a mesoporous catalyst in dielectric discharge plasmas. *Plasma Sources Sci. Technol.* **2017**, *26*, No. 054002.
- (52) Van Durme, J.; Dewulf, J.; Sysmans, W.; Leys, C.; Langenhove, V. Efficient toluene abatement in indoor air by a plasma catalytic hybrid system. *Appl. Catal., B* **2007**, *74*, 161–169.
- (53) Bogaerts, A.; Zhang, Q. Z.; Zhang, Y. R.; Laer, K. V.; Wang, W. Burning questions of plasma catalysis: Answers by modeling. *Catal. Today* **2019**, *337*, 3–14.
- (54) Vakili, R.; Gholami, R.; Stere, C. E.; Chasai, S.; Chen, H.; Holmes, S. M.; Jiao, Y.; Hardacre, C.; Fan, X. Plasma-assisted catalytic dry reforming of methane (DRM) over metal-organic frameworks (MOFs)-based catalysts. *Appl. Catal., B* **2020**, *260*, 118195.
- (55) Ashok, J.; Blan, Z.; Wang, Z.; Kawi, S. Ni-phyllsilicate structure derived Ni-SiO<sub>2</sub>-MgO catalysts for bi-reforming applications: Acidity, basicity and thermal stability. *Catal. Sci. Technol.* **2018**, *8*, 1730.
- (56) Yao, D.; Yang, H.; Chen, H.; Williams, P. T. Co-precipitation, impregnation and so-gel preparation of Ni catalysts for pyrolysis-catalytic steam reforming of waste plastics. *Appl. Catal., B* **2018**, *239*, 565–577.
- (57) Kim, H. H.; Teramoto, Y.; Negishi, N.; Ogata, A. A multidisciplinary approach to understand the interactions of non-thermal plasma and catalyst: A Review. *Catal. Today* **2015**, *256*, 13–22.
- (58) Chawdhury, P.; Wang, Y.; Ray, D.; Mathieu, S.; Wang, N.; Harding, J.; Bin, F.; Tu, X.; Challapalli, S. A promising plasma-catalytic approach towards single-step methane conversion to oxygenates at room temperature. *Appl. Catal., B* **2021**, *284*, 119735.
- (59) Jo, S.; Kim, T.; Lee, D. H.; Kang, W. S.; Song, Y. H. Effect of the electric conductivity of a catalyst on methane activation in a dielectric barrier discharge Reactor. *Plasma Chem. Plasma Process.* **2014**, *34*, 175–186.
- (60) Alayat, A.; Echeverria, E.; Sotoudehnikarani, F.; McLlroy, D. N.; McDonald, A. G. Alumina coated silica nanosprings (ns) support based cobalt catalysts for liquid hydrocarbon fuel production from syngas. *Materials (Basel, Switzerland)* **2019**, *12*, 1810.
- (61) Goujard, V.; Tatibouët, J. M.; Batiot-Dupeyrat, C. Use of a non-thermal plasma for the production of synthesis gas from biogas. *Appl. Catal., A* **2009**, *353*, 228–235.
- (62) Liu, C.-J.; Xue, B.; Eliasson, B.; He, F.; Li, Y.; Xu, G. H. Methane Conversion to Higher Hydrocarbons in the Presence of Carbon Dioxide Using Dielectric-Barrier Discharge Plasmas. *Plasma Chem. Plasma Process.* **2001**, *21*, 301–310.
- (63) Chen, G.; Snyders, R.; Britun, N. CO<sub>2</sub> conversion using catalyst-free and catalyst-assisted plasma-processes: Recent progress and understanding. *J. CO<sub>2</sub> Util.* **2021**, *49*, 101557.
- (64) Tao, K.; Ohta, N.; Liu, G.; Yoneyama, Y.; Wang, T.; Tsubaki, N. Plasma enhanced catalytic reforming of biomass tar model compound to syngas. *Fuel* **2013**, *104*, 53–57.
- (65) Zeng, Y.; Mei, D.; Tu, X., *Plasma-catalytic dry reforming of CH<sub>4</sub> and CO<sub>2</sub>: effect of bimetallic catalysts*, in 22nd International Symposium on Plasma Chemistry. : Antwerp: Belgium, 2015.
- (66) Zhang, A. J.; Zhu, A. M.; Guo, J.; Xu, Y.; Shi, C. Conversion of greenhouse gases into syngas via combined effects of discharge activation and catalysis. *Chem. Eng. J.* **2010**, *156*, 601–606.
- (67) Bogaerts, A.; Tu, X.; Whitehead, J. C.; Centi, G.; Lefferts, L.; Guitella, O.; Azzolina-Jury, F.; Kim, H. H.; Murphy, A. B.; Schneider, W. F.; Nozaki, T.; Hicks, J. C.; Rousseau, A.; Thevenet, F.; Khacef, A.; Carreon, M. The 2020 plasma catalysis roadmap. *J. Phys. D: Appl. Phys.* **2020**, *53*, 443001.